Phase diagram of spin-$\frac{1}{2}$ bosons in a one-dimensional optical lattice

L. de Forges de Parny,[1] M. Traynard,[1] F. Hébert,[1] V. G. Rousseau,[2] R. T. Scalettar,[3] and G. G. Batrouni[1,4,*]

[1]*INLN, Université de Nice-Sophia Antipolis, CNRS, 1361 Route des Lucioles, F-06560 Valbonne, France*

[2]*Department of Physics and Astronomy, Louisiana State University, Baton Rouge, Louisiana 70803, USA*

[3]*Physics Department, University of California, Davis, Davis, California 95616, USA*

[4]*Centre for Quantum Technologies, National University of Singapore, 2 Science Drive 3, Singapore 117542*

(Received 17 September 2010; published 3 December 2010)

Systems of two coupled bosonic species are studied using mean field theory and the quantum Monte Carlo method. The phase diagram is characterized on the basis of both the mobility of the particles (Mott insulating or superfluid) and whether or not the system is magnetic (different populations for the two species). The phase diagram is shown to be population balanced for negative spin-dependent interactions, regardless of whether it is insulating or superfluid. For positive spin-dependent interactions, the superfluid phase is always polarized, and the two populations are imbalanced. However, the Mott-insulating phase with even commensurate filling always has balanced populations. In contrast, the Mott phase with odd commensurate filling has balanced populations in a very strong interaction and polarizes as the interaction gets weaker while still in the Mott phase.

DOI: 10.1103/PhysRevA.82.063602 PACS number(s): 03.75.Mn, 05.30.Jp, 03.75.Hh, 75.10.Jm

I. INTRODUCTION

When ultracold bosonic atoms with internal degrees of freedom, for example, ^{87}Rb or ^{23}Na in the $F = 1$ hyperfine state, are confined in magneto-optical traps, the magnetic field aligns the spins and the system behaves effectively as one of spin-0 particles. Progress in purely optical trapping techniques now allows the confinement of these atoms with their full spin degrees of freedom present [1,2], which permits the study of the interplay between magnetism and superfluidity. In such systems, in addition to the usual spin-independent contact interaction, there are spin-dependent terms [3] and, also, longer-range interactions [4]. Mean field calculations [3] in the absence of long-range interactions show that the interactions can be ferromagnetic (e.g.,^{87}Rb) or antiferromagnetic (e.g., ^{23}Na), depending on the relative magnitudes of the scattering lengths in the singlet and quintuplet channels. When loaded in an optical lattice, the system is governed by an extended Hubbard Hamiltonian with spin-dependent and spin-independent terms. The phase diagram in the mean field and variational approximations has been calculated at zero [5–8] and at finite [8] temperature.

The overall picture emerging from these calculations is that in the ferromagnetic case, that is, a negative spin-dependent interaction, the system is in a Mott-insulating (MI) phase when the filling is commensurate with the lattice size and the repulsive contact interaction is strong enough. When this interaction is weaker, or when the particle filling is incommensurate, the system is in a ferromagnetic superfluid (SF) phase. SF-MI transitions in the ground state are all expected to be continuous. Furthermore, all Mott lobes shrink, and eventually disappear, as the ratio of the spin-dependent interaction to the spin-independent one increases. These predictions have been confirmed for the one-dimensional case with quantum Monte Carlo (QMC) simulations [9].

The phase diagram for the antiferromagnetic case also has MI lobes at commensurate fillings and strong coupling and an SF phase at weak coupling or incommensurate fillings. However, the natures of the SF phase and the MI-SF transitions are different. In this case, the SF phase is "polar": Superfluidity is carried either by the $S_z = 0$ component or by the $S_z = \pm 1$ components. Furthermore, Mott lobes of odd order are expected to be nematic in two and three dimensions and dimerized in one dimension [5]. The MI-SF transition into these odd Mott lobes is generally expected to be continuous. In even Mott lobes, the bosons are predicted to be in a singlet state, which is expected to increase the stability of the MI phase. This transition from nonsinglet SF to singlet MI phase is argued to render the transition into even Mott lobes of first order. Density matrix renormalization group [10,11] and QMC [12] calculations for one-dimensional systems have confirmed the dimerized nature of odd lobes and determined the phase diagram. Further QMC work [9] presented evidence of singlet formation in even lobes but did not find clear evidence of first-order phase transitions.

A related model is obtained by coupling degenerate atomic ground states and degenerate excited states (see next section) to yield a system of two bosonic species sometimes referred to as spin-1/2 bosons [13,14]. As for the full spin-1 case, the spin-dependent interaction can be ferromagnetic or antiferromagnetic. Mean field analysis of this model [13] yielded phase diagrams which are rather similar to the spin-1 case. In this paper we present an extension of previous mean field treatments [13] which yields a better qualitative agreement with exact QMC simulations, which we also present for the one-dimensional system. The paper is organized as follows: In Sec. II the Hamiltonian of two bosonic species is presented. The mean field phase diagram is discussed in Sec. III. Finally, in Sec. IV, QMC calculations on one-dimensional lattices verify the qualitative conclusions of the mean field theory (MFT), but provide quantitatively accurate values for the phase boundaries.

II. TWO-BOSONIC-SPECIES HAMILTONIAN

We follow Ref. [13] and consider a system of neutral polarizable bosonic atoms with three degenerate internal ground

*george.batrouni@inln.cnrs.fr

states ($F_g = 1$) and excited states ($F_e = 1$) characterized by the magnetic quantum number $S_z = 0, \pm 1$. The atoms are loaded in a d-dimensional optical lattice produced by counterpropagating laser beams. As explained in Ref. [13], in addition to generating the optical lattice, the lasers can be used to couple the internal ground and excited states by V and Λ transitions, leading to two sets of orthogonal Bloch eigenmodes denoted, respectively, 0 and Λ [13]. The resulting Bose-Hubbard Hamiltonian is given by

$$H = -t \sum_{\langle i,j\rangle,\sigma} (a^\dagger_{\sigma i} a_{\sigma j} + a^\dagger_{\sigma j} a_{\sigma i}) + \frac{U_0}{2} \sum_{\sigma,i} \hat{n}_{\sigma i}(\hat{n}_{\sigma i} - 1) + \frac{U_2}{2} \cos(\delta\phi) \sum_i (a^\dagger_{0i} a^\dagger_{0i} a_{\Lambda i} a_{\Lambda i} + a^\dagger_{\Lambda i} a^\dagger_{\Lambda i} a_{0i} a_{0i}) + (U_0 + U_2) \sum_i \hat{n}_{0i} \hat{n}_{\Lambda i} - \mu \sum_{\sigma,i} \hat{n}_{\sigma i}, \quad (1)$$

where $a^\dagger_{\sigma i}$ ($a_{\sigma i}$) creates (annihilates) a particle of "spin" $\sigma = 0, \Lambda$ on site i, $U_0 > 0$ is the spin-independent contact repulsion term, and U_2 is the spin-dependent interaction term. The number operator $\hat{n}_{\sigma i}$ counts the number of particles of type σ on site i, and μ is the chemical potential. We take the hopping parameter $t = 1$ to set the energy scale. The phase difference, $\delta\phi = 2(\phi_0 - \phi_\Lambda)$, gives the relative global phase between the two species. Equation (1) is the same as Eq. (9) in Ref. [13] after one uses Eqs. (13) and (15) in that reference. The relative phase, $(\phi_0 - \phi_\Lambda)$, was then determined by the requirement that the total energy be minimized. It was argued in Ref. [13] that since U_2 can be positive or negative, the way to minimize the energy is to have the coupling in the third term in Eq. (1) be of the form $-|U_2|/2$. This gives $\phi_0 = \phi_\Lambda$ for $U_2 < 0$ and $\phi_0 = \phi_\Lambda \pm \pi/2$ for $U_2 > 0$. The Hamiltonian then becomes

$$H_1 = -t \sum_{\langle i,j\rangle,\sigma} (a^\dagger_{\sigma i} a_{\sigma j} + a^\dagger_{\sigma j} a_{\sigma i}) + \frac{U_0}{2} \sum_{\sigma,i} \hat{n}_{\sigma i}(\hat{n}_{\sigma i} - 1) - \frac{|U_2|}{2} \sum_i (a^\dagger_{0i} a^\dagger_{0i} a_{\Lambda i} a_{\Lambda i} + a^\dagger_{\Lambda i} a^\dagger_{\Lambda i} a_{0i} a_{0i}) + (U_0 + U_2) \sum_i \hat{n}_{0i} \hat{n}_{\Lambda i} - \mu \sum_{\sigma,i} \hat{n}_{\sigma i}. \quad (2)$$

However, this is not the only possible solution: The sign of the third term has no effect on the energy, and the Hamiltonian obtained by putting $\phi_0 = \phi_\Lambda$ for both U_2 positive and U_2 negative,

$$H_2 = -t \sum_{\langle i,j\rangle,\sigma} (a^\dagger_{\sigma i} a_{\sigma j} + a^\dagger_{\sigma j} a_{\sigma i}) + \frac{U_0}{2} \sum_{\sigma,i} \hat{n}_{\sigma i}(\hat{n}_{\sigma i} - 1) + \frac{U_2}{2} \sum_i (a^\dagger_{0i} a^\dagger_{0i} a_{\Lambda i} a_{\Lambda i} + a^\dagger_{\Lambda i} a^\dagger_{\Lambda i} a_{0i} a_{0i}) + (U_0 + U_2) \sum_i \hat{n}_{0i} \hat{n}_{\Lambda i} - \mu \sum_{\sigma,i} \hat{n}_{\sigma i}, \quad (3)$$

yields exactly the same free energy as Eq. (2). For the $U_2 < 0$ case, this is obvious since Eq. (2) is identical to Eq. (3). For $U_2 > 0$, this can be seen by writing the partition function, $Z = \mathrm{Tr}\, e^{-\beta H}$, and noting that if we expand the exponential in powers of the term in question, only even powers will contribute. In fact, for $U_2 > 0$, one can transform Eq. (2) into Eq. (3) by a simple phase transformation, $a_{0i} \to a_{0i} e^{i\pi/2}$. Therefore, both Eqs. (2) and (3) are valid and yield the same results for energies and all other quantities that are invariant under the preceding phase transformation when examined with an exact method such as QMC. This is not necessarily so when approximations are made, as we see in the next section.

III. MEAN FIELD PHASE DIAGRAMS

In this section we revisit the mean field phase diagrams of the model governed by Eqs. (2) and (3). This is implemented by first writing the identity,

$$a^\dagger_{\sigma i} a_{\sigma j} = (a^\dagger_{\sigma i} - \langle a^\dagger_\sigma \rangle)(a_{\sigma j} - \langle a_\sigma \rangle) + \langle a^\dagger_\sigma \rangle a_{\sigma j} + a^\dagger_{\sigma i} \langle a_\sigma \rangle - \langle a^\dagger_\sigma \rangle \langle a_\sigma \rangle. \quad (4)$$

The SF order parameter is $\langle a^\dagger_\sigma \rangle = \langle a_\sigma \rangle \equiv \psi_\sigma$ and is taken to be real and uniform, that is, independent of the position. The first term in Eq. (4) is a small fluctuation and is ignored; substituting the remaining terms in Eq. (2) reduces H_1 to the sum of single-site Hamiltonians,

$$H_{\mathrm{MF1}} = -2td \sum_\sigma \left[\psi_\sigma (a^\dagger_\sigma + a_\sigma) - \psi^2_\sigma\right] + \frac{U_0}{2} \sum_\sigma \hat{n}_\sigma(\hat{n}_\sigma - 1) - \frac{|U_2|}{2} (a^\dagger_0 a^\dagger_0 a_\Lambda a_\Lambda + a^\dagger_\Lambda a^\dagger_\Lambda a_0 a_0) + (U_0 + U_2)\hat{n}_0 \hat{n}_\Lambda - \mu \sum_\sigma \hat{n}_\sigma; \quad (5)$$

and from Eq. (3), H_2 becomes

$$H_{\mathrm{MF2}} = -2td \sum_\sigma \left[\psi_\sigma (a^\dagger_\sigma + a_\sigma) - \psi^2_\sigma\right] + \frac{U_0}{2} \sum_\sigma \hat{n}_\sigma(\hat{n}_\sigma - 1) + \frac{U_2}{2} (a^\dagger_0 a^\dagger_0 a_\Lambda a_\Lambda + a^\dagger_\Lambda a^\dagger_\Lambda a_0 a_0) + (U_0 + U_2)\hat{n}_0 \hat{n}_\Lambda - \mu \sum_\sigma \hat{n}_\sigma. \quad (6)$$

The mean field solution is obtained by taking matrix elements of these Hamiltonians in a truncated basis of single-site occupation number states $|\, n_0\, n_\Lambda \rangle$, diagonalizing the resulting matrix and then minimizing the lowest eigenvalue with respect to the order parameters ψ_σ. The basis is truncated for large particle numbers (typically $n_0 = n_\Lambda = 12$) to obtain results independent of the truncation. This gives the order parameter of the ground state and its eigenvector. The SF density is given by

$$\rho_s = \psi^2_0 + \psi^2_\Lambda. \quad (7)$$

A. Ferromagnetic case: $U_2 < 0$

The two mean field Hamiltonians, H_{MF1} and H_{MF2} are identical for the ferromagnetic case, $U_2 < 0$, and their ground state was studied in Ref. [13]. At commensurate filling and strong interaction (small t/U_0), the energy has one minimum, at $\psi_0 = \psi_\Lambda = 0$, corresponding to the MI phase. Figure 1(a) shows this for the Mott phase with two particles per site, $\rho = 2$. For any noncommensurate filling and for commensurate filling at weak coupling, there are four symmetric and degenerate

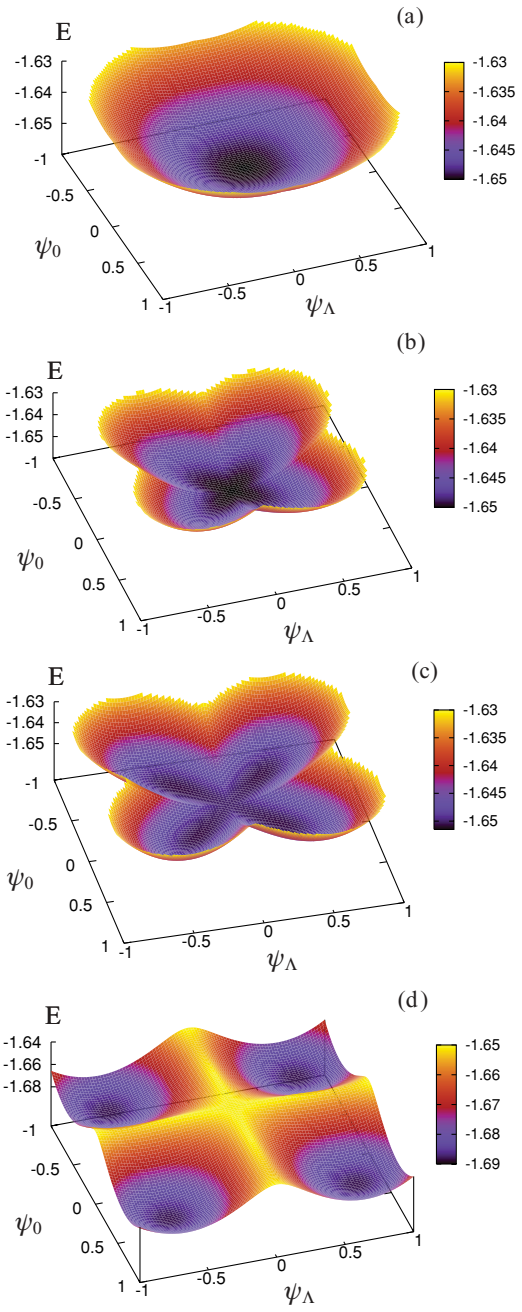

FIG. 1. (Color online) Ground-state energy E, given by Eq. (5) or (6) in the ferromagnetic case, $U_2 = -0.1U_0$ at $\rho = 2$ ($\mu/U_0 = 1.3$). (a) $U_0 = 100t$; the system is in the MI phase. (b) $U_0 = 25t$; the system is in the MI phase close to the transition into the SF phase. (c) $U_0 = 20t$; the system has just made the transition into the SF phase. The minimum has changed continuously from $\psi_0 = \psi_\Lambda = 0$ to four degenerate minima at nonzero values of the order parameters. (d) $U_0 = 12.5t$; the system is in the SF phase. Note the degenerate symmetric minima in the SF case, $|\psi_0| = |\psi_\Lambda| \neq 0$. This figure agrees with Fig. 2 in Ref. [13].

minima with $|\psi_0| = |\psi_\lambda| \neq 0$ corresponding to the SF phase, Fig. 1(d). For later reference, we emphasize that the SF phase is symmetric in the two particle species, $|\psi_0| = |\psi_\lambda|$. Figures 1(b) and 1(c) show how the minimum at $\psi_0 = \psi_\Lambda = 0$ transforms continuously into four degenerate minima shown

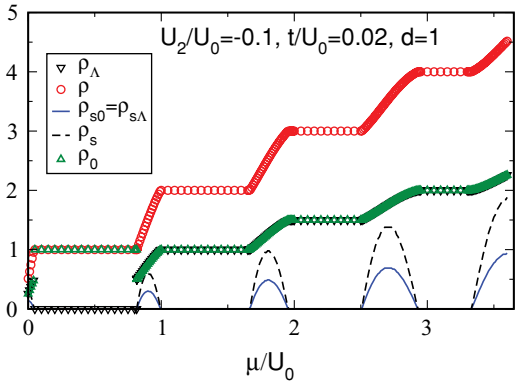

FIG. 2. (Color online) Densities of the two species ρ_0 and ρ_Λ, total density $\rho = \rho_0 + \rho_\Lambda$, and the corresponding superfluid densities as functions of μ/U_0. In the ferromagnetic case, $\rho_{s0} = \rho_{s\Lambda}$ and $\rho_0 = \rho_\Lambda$ except in the first Mott lobe. The reason is that the particles do not interact, and so there is no possibility of conversion of one species to another.

in Fig. 1(d) as the interaction gets weaker. The same behavior is seen for the MI phase at all other commensurate fillings.

The MFT phase diagram is obtained by repeating the preceding calculation for many values of the chemical potential μ and the interaction U_0 (always keeping U_2/U_0 constant). In the no-hopping limit, $t/U_0 \to 0$, it is easy to see that when μ satisfies the condition

$$(n-1)(U_0 - |U_2|) < \mu < n(U_0 - |U_2|), \tag{8}$$

the system is in an MI phase with n bosons per site. As t/U_0 increases, always keeping $|U_2|/U_0$ constant, the MI region shrinks and eventually disappears, giving the familiar Mott lobes. Outside the MI region the system is SF. Note that U_2 has the effect of shrinking the bases of all the Mott lobes (Fig. 3): When $|U_2| = U_0$ the lobes disappear completely. In Fig. 2 we show mean field results for the densities ρ_0 and ρ_Λ of the two species, the total density $\rho = \rho_0 + \rho_\Lambda$, and the corresponding SF densities as functions of μ for fixed $t/U_0 = 0.02$ and $U_2/U_0 = -0.1$. We see that all compressible regions, $\kappa = \partial\rho/\partial\mu \neq 0$, are SF, while the incompressible plateaus, $\kappa = 0$, are not SF; they are MI. The absence of discontinuous jumps in any of the densities as the system enters the MI phase indicates that the transitions are continuous, as also discussed in Ref. [13]. We also remark that since in the ferromagnetic case we have $|\psi_0| = |\psi_\Lambda|$, then $\rho_{s0} = \rho_{s\Lambda}$ and $\rho_0 = \rho_\Lambda$ everywhere except in the first Mott plateau where one of the species has 0 density, in this case $\rho_\Lambda = 0$. The reason the first Mott region behaves in this way is that, for the two species to interconvert, the particles have to meet and interact. In the MI phase, the particles do not hop between the sites, with the consequence that in the first MI phase there is only one particle per site and no way to interconvert the species. The phase diagram is shown in Fig. 3.

B. Antiferromagnetic case: $U_2 > 0$

In the antiferromagnetic case, $U_2 > 0$, the Hamiltonians Eqs. (5) and (6) are no longer identical. Reference [13] performed the mean field calculation using Eq. (5) and found that in the MI phase, the energy has one minimum

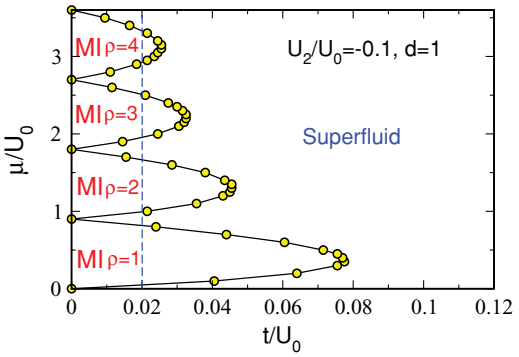

FIG. 3. (Color online) Phase diagram given by the mean field Hamiltonian, Eq. (5) or (6), in the ferromagnetic case $U_2 = -0.1U_0$. Note the shrinking of the bases of all lobes by $|U_2|/U_0$. The dashed vertical line shows where the cut in Fig. 2 was taken.

at $\psi_0 = \psi_\Lambda = 0$. As the system is taken closer to the tip of the Mott lobe, the energy develops local minima (Fig. 6 in Ref. [13]); these local minima become global minima in the SF phase, indicating that the MI-SF transition can be of first order. Furthermore, it was found that there is a continuum of degenerate minima at nonzero ψ_0 and ψ_Λ (Fig. 6 in Ref. [13]).

Doing the mean field calculation with Eq. (6) leads to results which are similar in some ways to the foregoing ones but different in very important aspects. First, for a given choice of t, U_0, U_2, and μ, we found that the two mean field Hamiltonians give the same ground-state energy in both the SF and the MI phases. Therefore, one cannot choose between them on this basis. In the MI phase, whether the filling is odd or even, Eq. (6) gives a ground-state energy with one minimum at $\psi_0 = \psi_\Lambda = 0$, as does Eq. (5). As the system is brought closer to the lobe tip, the behavior depends on whether the filling in the Mott phase is odd or even. Odd filling is similar to the ferromagnetic case: The global minimum at $\psi_0 = \psi_\Lambda = 0$ transforms continuously into four degenerate minima with a nonvanishing order parameter. However, in this antiferromagnetic case, the minima lie on the ψ_0 and ψ_Λ axes: Either $\psi_0 = 0$ while $\psi_\Lambda \neq 0$ or $\psi_0 \neq 0$ while $\psi_\Lambda = 0$. This means that in the SF phase, the SF density is composed entirely of one species: Either ($\rho_s = \rho_{s0}$, $\rho_{s\Lambda} = 0$) or ($\rho_{s0} = 0$, $\rho_s = \rho_{s\Lambda}$). Our result differs from that in Ref. [13], where a continuum of degenerate minima was found in the SF phase.

If the filling of the MI phase is even, then as the system approaches the tip of the lobe, decreasing the interaction U_0, *local* minima develop at nonzero ψ_0 *or* ψ_Λ: With Eq. (6) the local minima do not form an axisymmetric continuum as they do with Eq. (5) (see Ref. [13]). As for the odd lobes just discussed, the minima lie either on the ψ_0 axis or on the ψ_Λ axis. This is illustrated in Fig. 4, which shows, for $\rho = 2$, the behavior of the energy minima as the interaction is reduced, taking the system from the MI to the SF phase. Figures 4(b) and 4(c) illustrate the behavior as the system is leaving the MI phase. First, local minima develop with a nonvanishing order parameter, indicating a metastable SF [Fig. 4(b)]. These local minima then become global for lower U_0, while the previously global minimum at the origin becomes local, indicating that the MI is now metastable [Fig. 4(c)]. Such behavior signals a first-order SF-MI transition for the even Mott phases. The

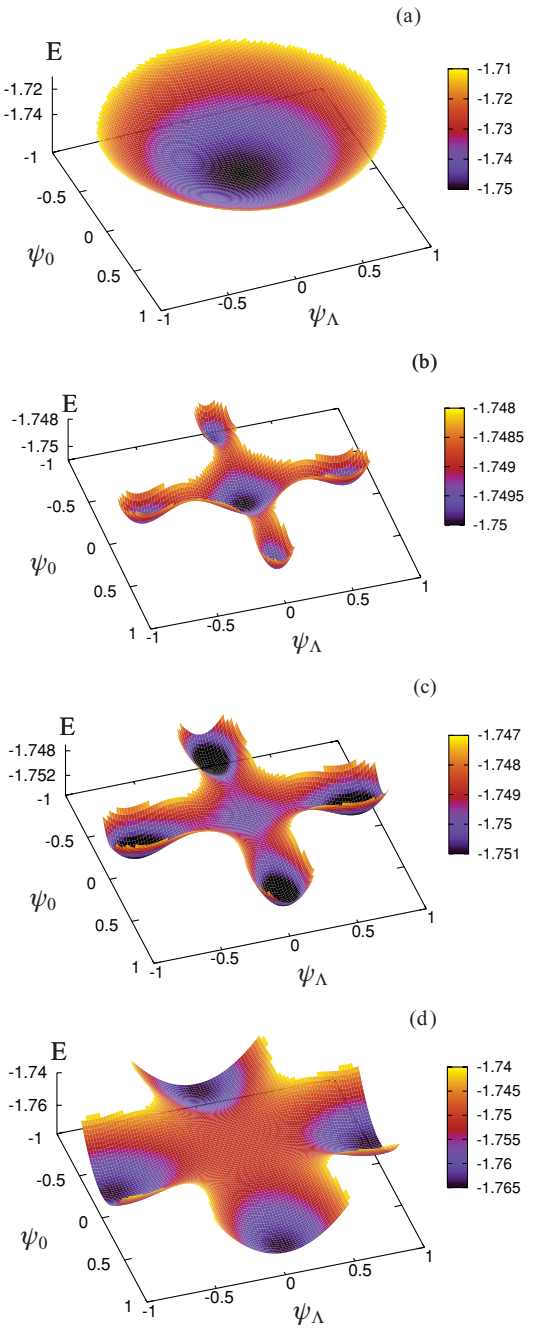

FIG. 4. (Color online) Ground-state energy given by Eq. (6) in the antiferromagnetic case, $U_2 = 0.1U_0$. (a) $U_0 = 33.3t$; the global minimum is at $\psi_0 = \psi_\Lambda = 0$ and the system is in the MI phase. (b) $U_0 = 12.5t$; local minima are at nonzero ψ_0 or ψ_Λ, indicating stable MI and metastable SF phases. (c) $U_0 = 12.2t$; global minima are at nonzero ψ_0 or ψ_Λ, indicating stable SF and metastable MI phases. (d) $U_0 = 11.11$; four degenerate global minima, indicating the system is in the SF phase.

nature of the transition is in agreement with Ref. [13] but not the nature of the SF phase. According to our mean field result, when the system is in the SF phase, superfludity is carried entirely by one species or the other, but not by both. This result is in marked contrast with that of the MFT based on Eq. (5) and is similar to the MFT prediction for the SF phase of the full spin-1 model [8] in the antiferromagnetic case.

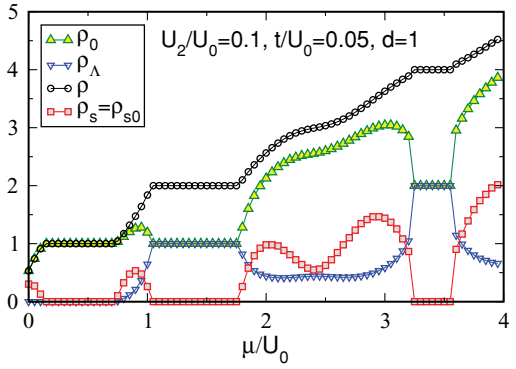

FIG. 5. (Color online) Densities of the two species ρ_0 and ρ_Λ, the total density, $\rho = \rho_0 + \rho_\Lambda$, and the corresponding superfluid densities as functions of μ/U_0 in the antiferromagnetic case. This cut is taken just outside the third lobe (see Fig. 6), so the compressibility, $\kappa = \partial\rho/\partial\mu$, does not quite vanish. Note the discontinuous transition into the fourth Mott lobe.

In Fig. 5 we show the densities of the two species, ρ_0 and ρ_Λ, the total density, $\rho = \rho_0 + \rho_\Lambda$, and the corresponding SF densities as functions of μ/U_0 in the antiferromagnetic case. Several features are noteworthy. The first, second, and fourth incompressible MI plateaus are clearly visible but the third plateau does not quite form. This is because the cut shown in Fig. 5 passes just outside the third Mott lobe; see the phase diagram in Fig. 6. As in the ferromagnetic case, the first Mott lobe is made of only one species, ρ_0 in this case. In the even Mott lobes we have $\rho_0 = \rho_\Lambda$, but nowhere else. In addition, superfluidity is carried entirely by one species; in this case $\rho_s = \rho_{s0}$ and $\rho_{s\Lambda} = 0$ even though $\rho_\Lambda \neq 0$. We also note that the transition into the fourth plateau is discontinuous: We see clearly the discontinuous jumps of ρ_0, ρ_Λ, and ρ_s as this plateau is approached. This is in agreement with the discussion of Fig. 4 and indicates that the system shown in Fig. 5 enters the fourth Mott lobe near its tip. This is confirmed in the full phase diagram (Fig. 6).

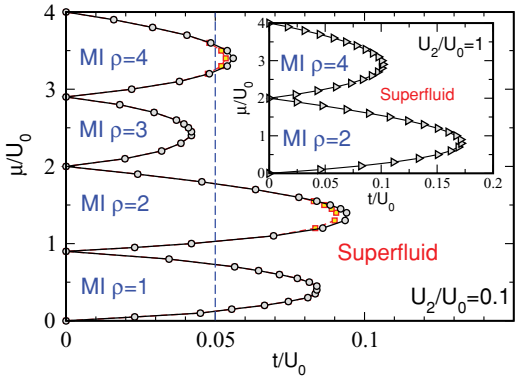

FIG. 6. (Color online) Mean field phase diagram given by Eq. (6) for $U_2/U_0 = 0.1$. The bases of the odd MI lobes are reduced by U_2/U_0; the phase transitions near the tips of the even lobes are first order. Regions between the squares and the circles around the tips of the even lobes denote regions where the SF (MI) phase is metastable while the MI (SF) phase is stable. Inset: Phase diagram for $U_2/U_0 = 1$; all odd MI lobes have vanished.

The phase diagram is obtained by calculating slices as in Fig. 5 for different values of μ and t/U_0 at fixed U_2/U_0. Figure 6 shows the mean field phase diagram for the case $U_2 = 0.1U_0$, while the inset shows it for $U_2 = U_0$. The boundaries of the phases do not depend much on whether one uses Eq. (5) or Eq. (6) for the mean field calculation. However, the nature of the SF phase depends crucially on which Hamiltonian is used, as already discussed. For the $U_2/U_0 = 0.1$ case and, more generally, for small U_2/U_0, the transition near the tip of even Mott lobes is first order, as discussed in connection with Figs. 5 and 6: The regions between the squares and the circles around the tips of the even Mott lobes in Fig. 6 denote the regions where the SF (MI) phase is metastable while the MI (SF) phase is stable. The lower the ratio U_2/U_0, the wider the first-order transition region. In contrast, when the ratio U_2/U_0 is high enough, there are no discontinuous transitions; only continuous transitions remain. The extreme case of $U_2 = U_0$, where all odd lobes disappear, is shown in the inset in Fig. 6.

IV. QUANTUM MONTE CARLO PHASE DIAGRAM

In this section we present the results of exact QMC simulations for the system governed by the Hamiltonian Eq. (2) or Eq. (3). As mentioned before, these two forms of the Hamiltonian are identical for $U_2 < 0$ and are equivalent for $U_2 > 0$ in that they are related by a simple phase rotation and do, in fact, give the same results in QMC simulations for all the quantities we examined.

For our simulations we use the stochastic Green function algorithm [15] with directed update [16]. This algorithm can be implemented in both the canonical and the grand canonical ensembles [17]. In this work we used mostly the canonical formulation, where we relate the density to the chemical potential using

$$\mu(N) = E(N+1) - E(N). \tag{9}$$

N is the total number of particles in a system with L lattice sites, and $E = \langle H \rangle$ is the total internal energy which is equal to the free energy in the ground state. Another very important quantity for characterizing the phases is the SF density, which is given by [18]

$$\rho_s = \frac{\langle W^2 \rangle}{2dt\beta L^{d-2}}, \tag{10}$$

in the single-species case where W is the winding number of the bosons. In the present case, there are two species of particles which can be converted into each other. Consequently, the relevant winding number is the total for the two species, and the SF density is then given by

$$\rho_s = \frac{\langle (W_0 + W_\lambda)^2 \rangle}{2dt\beta L^{d-2}}. \tag{11}$$

A. Ferromagnetic case: $U_2 < 0$

We start with ferromagnetic case, $U_2 < 0$. As we did with the MFT, we calculate the phase diagram in the $(\mu/U_0, t/U_0)$ plane at a fixed ratio U_2/U_0. We take $|U_2|/U_0 = 0.1$ because

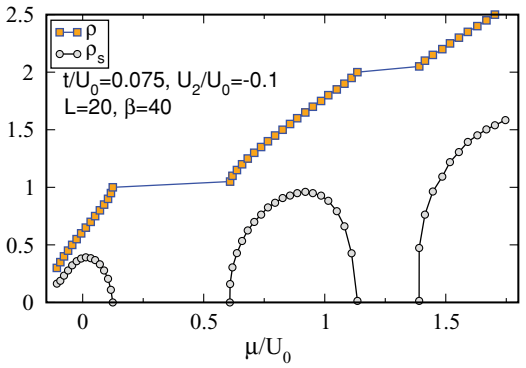

FIG. 7. (Color online) Total particle density ρ and superfluid density ρ_s as functions of the chemical potential μ. The first two Mott plateaus are clearly visible.

we want to use the same value for the ferro- and the antiferromagnetic cases, and in the latter case, MFT predicts first-order transitions for the even Mott lobes for this value. With $U_2/U_0 = -0.1$, we study the SF-MI transition as the chemical potential (or density) is varied by calculating ρ versus μ slices for different fixed t/U_0. Using the canonical algorithm, this is done by incrementing the number of bosons one particle at a time, doing the simulation, and then calculating the chemical potential μ using Eq. (9). Figure 7 shows such a slice at $t/U_0 = 0.075$ and clearly exhibits the first two incompressible Mott plateaus. Furthermore, we see that when the system is compressible, it is also SF, $\rho_s \neq 0$. In the Mott plateaus, the SF density vanishes, $\rho_s = 0$.

Next, we study the SF-MI transition at fixed commensurate filling, integer ρ, as the coupling t/U_0 is changed. This exhibits the behavior of the transition at the tips of the Mott lobes. In Fig. 8 we show the SF density ρ_s versus t/U_0 for $\rho = 1, 2$. We see that in both cases, $\rho = 1$ [Fig. 8(a)] and $\rho = 2$ [Fig. 8(b)], ρ_s changes continuously as predicted by MFT.

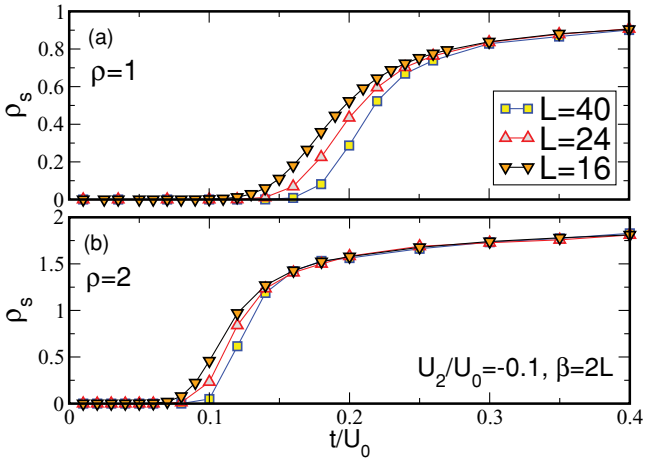

FIG. 8. (Color online) Superfluid density ρ_s as a function of t/U_0 in the first (a) and second (b) Mott lobes. No evidence of a discontinuous jump can be seen as the system size increases; transitions are continuous.

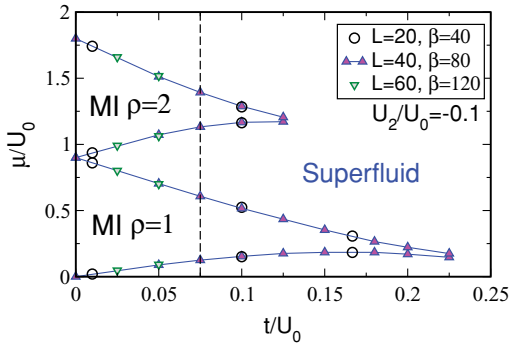

FIG. 9. (Color online) QMC phase diagram of the ferromagnetic system with $U_2/U_0 = -0.1$. All Mott lobes shrink by $\delta\mu/U_0 = 0.1$ at their bases as in the mean field case (Fig. 3). Note, however, that unlike the rounded lobes in the mean field case, the lobes here end in cusps. This is strong evidence that the gap vanishes exponentially, a behavior characteristic of the KT universality class of the two-dimensional XY model. This phase diagram is very similar to that of the full spin-1 model in Ref. [9]. The dashed vertical line indicates where the cut in Fig. 7 was taken.

The phase diagram is obtained by calculating ρ versus μ scans for several t/U_0 values, as shown in Fig. 9. System sizes $L = 20$, 40, and 60 were used, showing very few finite-size effects for the gap. We remark that, as expected, the Mott lobes shrink by $\delta\mu/U_0 = 0.1$ at their bases and will disappear completely for $|U_2| = U_0 = 1$. While the QMC and MFT phase diagrams are similar qualitatively, the Mott lobes given by the MFT are rounded, while those given by exact QMC end in cusps. This is consistent with a critical point at the tip in the universality class of the two-dimensional XY model, which is expected from general scaling arguments [20] and was first observed in QMC in Ref. [21].

Finally, in Fig. 10 we show the density distribution for total density $\rho = 2$ as t/U_0 is increased, taking the system from deep in the second Mott lobe into the SF phase as in Fig. 8(b). We find that the distributions for the 0 and Λ species are identical and that the peak is at $\rho_0 = \rho_\Lambda = 1$,

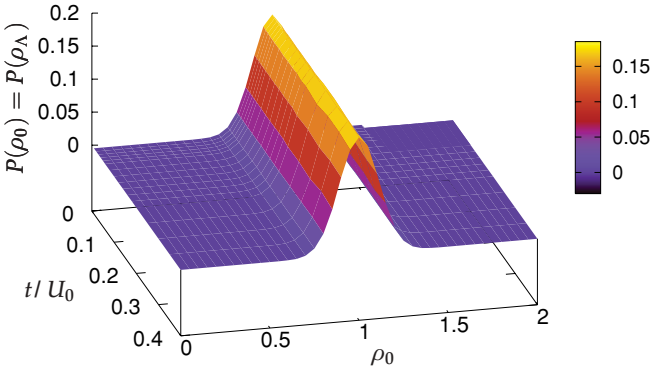

FIG. 10. (Color online) Density distribution of the 0 particles as a function of t/U_0. The total density is $\rho = 2$ and the values of t/U_0 take the system from deep in the second Mott lobe to the superfluid phase. The distributions of the two species, 0 and Λ, are identical and peak at a value of $\rho/2 = 1$. Compare with Fig. 15.

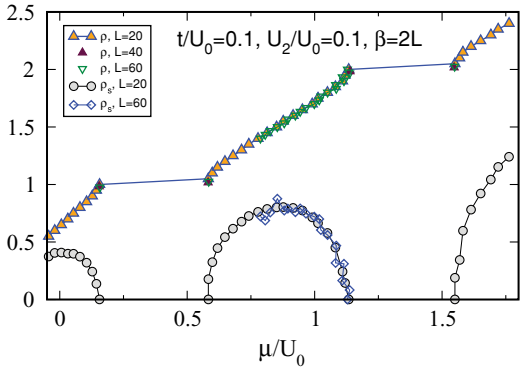

FIG. 11. (Color online) Total density ρ as a function of the chemical potential μ, showing the first two incompressible Mott phases. Also shown is the superfluid density ρ_s in the compressible phases.

even though the initial state for these simulations was chosen to be $\rho_0 = 2$, $\rho_\Lambda = 0$: In the ferromagnetic case, the density distributions, $P(\rho_0)$ and $P(\rho_\Lambda)$, are the same in both the MI and the SF phases. This means that the SF density is carried by both particles. The same behavior was found for $\rho = 1$. This is compared to the antiferromagnetic case in the following section.

B. Antiferromagnetic case: $U_2 > 0$

The phase diagram in the antiferromagnetic case, $U_2 > 0$, is determined in the same way as for $U_2 < 0$: We calculate slices of ρ versus μ for various values of t/U_0, keeping $U_2/U_0 > 0$ fixed. Such a slice going through the first two Mott plateaus is shown in Fig. 11. As in the ferromagnetic case, we see that the compressible phase is SF, $\rho_s \neq 0$. MFT predicts that the SF-MI transition near the tip of the even Mott lobes is first order. We found no evidence of that; ρ_s vanishes continuously as a function of μ as the MI phase is approached. In the canonical ensemble, as we have here, first-order transitions

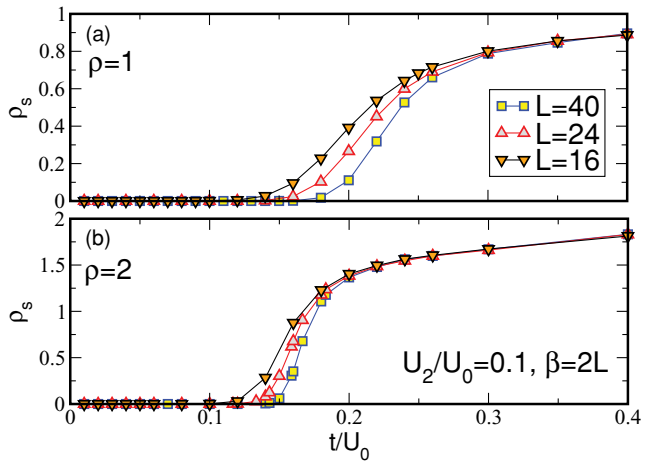

FIG. 12. (Color online) Superfluid (SF) density ρ_s as a function of t/U_0 in the first (a) and second (b) Mott lobes for the antiferromagnetic case. No evidence of a discontinuous jump can be seen as the system size increases. SF-MI transitions at the tips of the Mott lobes are continuous.

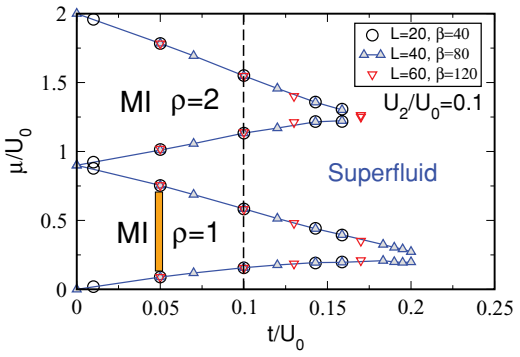

FIG. 13. (Color online) Phase diagram in the antiferromagnetic case with data from three lattice sizes. Finite-size effects are small. Note that, as expected, the lower boundary of the base of the second lobe shifts down by $U_2/U_0 = 0.1$ but the upper boundary does not. When $U_2/U_0 = 1$, all odd-order lobes disappear and only even-order ones remain. The vertical dashed line indicates where the ρ-versus-μ cut in Fig. 11 was taken. The vertical (orange) bar at $t/U_0 = 0.05$ in the first lobe indicates where this Mott phase polarizes. See discussion of Fig. 14 in text.

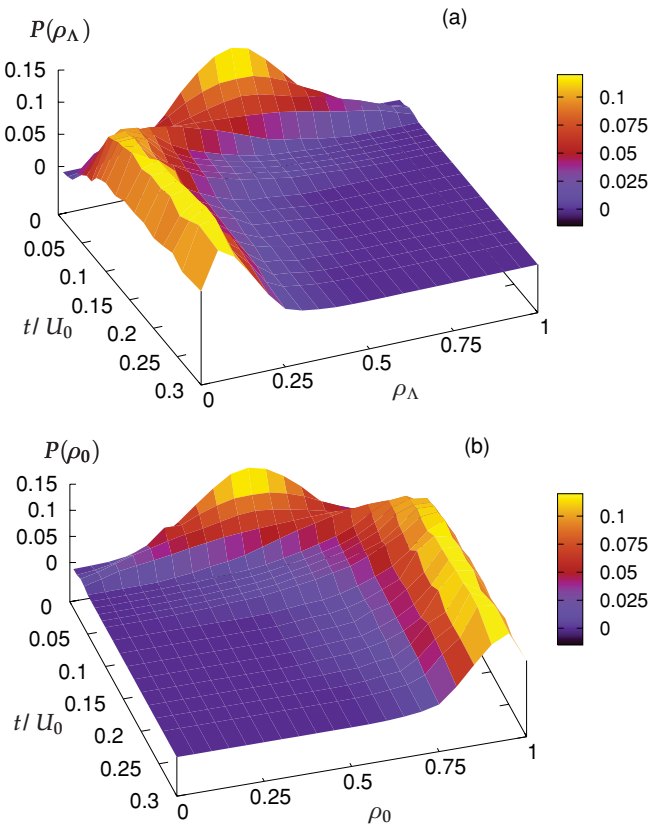

FIG. 14. (Color online) Density distribution of Λ (a) and 0 (b) particles as functions of t/U_0. The system size is $L = 40$, $\beta = 80$, and the total density is $\rho = 1$. The values of t/U_0 take the system from deep in the first Mott lobe to the superfluid phase. Inside the Mott lobe, the system is unpolarized, $P(\rho_0) = P(\rho_\Lambda)$, for $t/U_0 < 0.05$ and both distributions peak at $\rho/2 = 0.5$. At $t/U_0 \approx 0.05$, while the system is still in the first Mott lobe, it polarizes: The peak of one distribution approaches the total density, $\rho = 1$, while the other approaches 0. We verified that the same behavior is observed for different system sizes. This transition in the Mott lobe is not predicted by MFT.

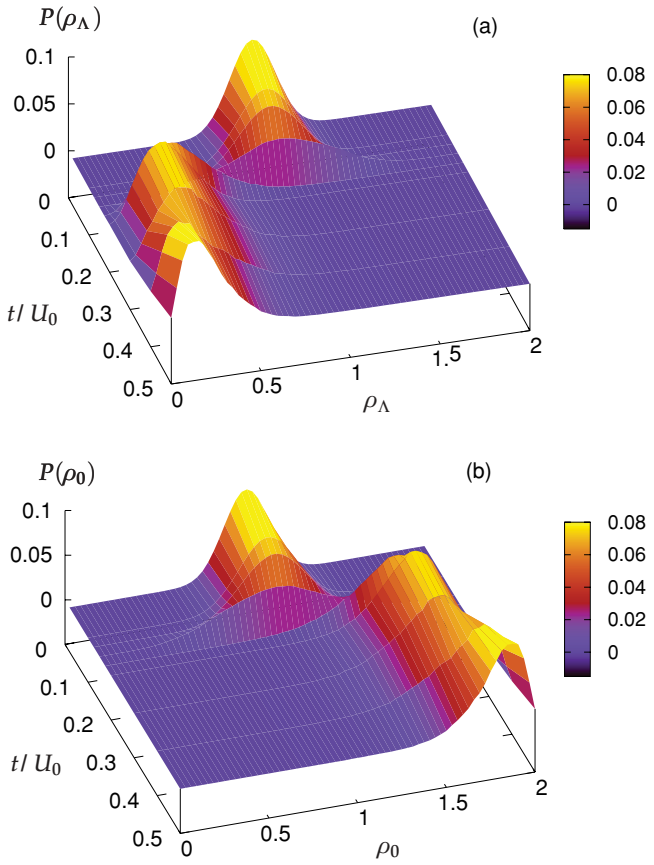

FIG. 15. (Color online) Density distribution of Λ (a) and 0 (b) particles as functions of t/U_0. The system size is $L = 64$, $\beta = 128$, and the total density is $\rho = 2$; the values of t/U_0 take the system from deep in the second Mott lobe to the superfluid phase. Inside the Mott lobe, $P(\rho_0) = P(\rho_\Lambda)$ and both distributions peak at $\rho/2 = 1$. As soon as the system leaves the Mott phase and becomes superfluid, it is polarized: The peak of one distribution approaches the total density, $\rho = 2$, while the other approaches 0. The superfluid phase is polarized as predicted by the MFT: The superfluidity is carried entirely by one species.

are signaled by regions of negative compressibility [22], $\kappa = \partial\rho/\partial\mu < 0$. We found that κ is always positive for all values of t/U_0, indicating that the SF-MI transition is not first order.

We confirm the nature of the SF-MI transition by studying the behavior of the SF density as a function of t/U_0 at a fixed total density $\rho = 1, 2$. Figure 12 shows ρ_s versus t/U_0 for the first and second Mott plateaus. In both cases ρ_s changes continuously as the system transitions from the MI to the SF phase, confirming that all SF-MI transitions in this model are continuous.

The phase diagram is obtained, as before, by calculating ρ versus μ for several values of t/U_0 and mapping out the Mott lobes. The resulting phase diagram for the first two lobes is shown in Fig. 13.

Finally, we show in Fig. 14 that the density distribution for total density $\rho = 1$ as t/U_0 is increased, taking the system from deep in the first Mott lobe into the SF phase. We see that for $t/U_0 < 0.05$, the system is unpolarized; the two populations have identical distributions which peak at $\rho_\Lambda = \rho_0 = 0.5$. At $t/U_0 \approx 0.05$, while the system is still deep in the Mott lobe (see Fig. 13), the system polarizes: The population of one species drops abruptly to near 0, while that of the other species increases to close to full filling. This polarization persists throughout the SF-MI transition. This transition inside the first Mott lobe is not predicted by MFT.

In Fig. 15 we show the density distributions in the second Mott lobe. Here we find that the system polarizes only when it transitions from the MI to the SF phase at $t/U_0 \approx 0.17$. Consequently, the SF phase in the antiferromagnetic phase is always polarized: The system is mostly populated by a single species, and consequently, superfluidity is carried by that one particle type. This behavior was predicted, qualitatively, by our mean field calculation and is very different from the behavior in the ferromagnetic case.

V. CONCLUSIONS

In this work, we have performed MFT calculations of the phase diagram of the spin-1/2 bosonic Hubbard model, Eqs. (2) and (3). These models, which are derived from the full spin-1 model, are equivalent when treated exactly, but we found that the MFT results depend on which Hamiltonian is used in the antiferromagnetic ($U_2 > 0$) case but are identical in the ferromagnetic case ($U_2 < 0$). In particular, a previous MFT result [13] found that the SF phase does not polarize spontaneously when $U_2 > 0$. Treating the mean field model more carefully, we found that the antiferromagnetic case, $U_2 > 0$, results in a spontaneously polarized SF phase. We then used exact QMC simulations to calculate the phase diagram for $U_2 < 0$ and $U_2 > 0$. For $U_2 < 0$, we found that the populations are balanced both in the SF and in the incompressible phases, in agreement with our mean field calculation and that of Ref. [13]. For $U_2 > 0$, we found that the SF phase is always polarized, with one species dominating the population: This confirms our MFT results and contradicts those in Ref. [13]. Throughout the second Mott lobe (and, presumably, for all even Mott lobes), the populations are balanced, again, in agreement with our mean field results. In contrast, for $t/U_0 < 0.05$ in the first Mott lobe, we found that the populations are balanced but that the system polarizes inside the Mott lobe at $t/U_0 \approx 0.05$. This is a new transition inside the Mott lobe and was not predicted previously by mean field calculations. It is plausible that this result generalizes to higher odd Mott lobes; at present, simulations are not feasible at the needed high densities and couplings. Finally, our MFT calculations and those in Ref. [13] both predict that when $U_2/U_0 > 0$ is small enough, the MI-SF transition is discontinuous near the tips of even Mott lobes. Our QMC results show this not to be the case; all the transitions are observed to be continuous.

ACKNOWLEDGMENTS

This work was supported by the CNRS–UC Davis EPOCAL LIA joint research grant, NSF Grant No. OISE-0952300, and ARO Grant No. W911NF0710576 with funds from the DARPA OLE Program. We thank A. Brothers for helpful insight.

[1] M. Vengalattore, S. R. Leslie, J. Guzman, and D. M. Stamper-Kurn, Phys. Rev. Lett. **100**, 170403 (2008).
[2] M. Vengalattore, J. Guzman, S. Leslie, F. Serwane, and D. M. Stamper-Kurn, Phys. Rev. A **81**, 053612 (2010).
[3] T.-L. Ho, Phys. Rev. Lett. **81**, 742 (1998).
[4] Jay D. Sau, S. R. Leslie, D. M. Stamper-Kurn, and Marvin L. Cohen, Phys. Rev. A **80**, 023622 (2009).
[5] A. Imambekov, M. Lukin, and E. Demler, Phys. Rev. A **68**, 063602 (2003); Phys. Rev. Lett. **93**, 120405 (2004).
[6] T. Kimura, S. Tsuchiya, and S. Kurihara, Phys. Rev. Lett. **94**, 110403 (2005).
[7] E. Demler and F. Zhou, Phys. Rev. Lett. **88**, 163001 (2002); M. Snoek and F. Zhou, Phys. Rev. B **69**, 094410 (2004).
[8] R. V. Pai, K. Sheshadri, and R. Pandit, Phys. Rev. B **77**, 014503 (2008).
[9] G. G. Batrouni, V. G. Rousseau, and R. T. Scalettar, Phys. Rev. Lett. **102**, 140402 (2009).
[10] M. Rizzi, D. Rossini, G. De Chiara, S. Montangero, and R. Fazio, Phys. Rev. Lett. **95**, 240404 (2005).
[11] S. Bergkvist, I. P. McCulloch, and A. Rosengren, Phys. Rev. A **74**, 053419 (2006).
[12] V. Apaja and O. F. Syljuåsen, Phys. Rev. A **74**, 035601 (2006).
[13] K. V. Krutitsky and R. Graham, Phys. Rev. A **70**, 063610 (2004); K. V. Krutitsky, M. Timmer, and R. Graham, *ibid.* **71**, 033623 (2005).
[14] S. Ashhab, J. Low Temp. Phys. **140**, 51 (2005).
[15] V. G. Rousseau, Phys. Rev. E **77**, 056705 (2008).
[16] V. G. Rousseau, Phys. Rev. E **78**, 056707 (2008).
[17] M. J. Wolak, V. G. Rousseau, C. Miniatura, B. Grémaud, R. T. Scalettar, and G. G. Batrouni, e-print arXiv:1004.4499v1.
[18] D. M. Ceperley and E. L. Pollock, Phys. Rev. B **39**, 2084 (1989).
[19] B. Capogrosso-Sansone, S. G. Söyler, N. V. Prokofév, and B. V. Svistunov, Phys. Rev. A **81**, 053622 (2010).
[20] M. P. A. Fisher, P. B. Weichman, G. Grinstein, and D. S. Fisher, Phys. Rev. B **40**, 546 (1989).
[21] G. G. Batrouni, R. T. Scalettar, and G. T. Zimanyi, Phys. Rev. Lett. **65**, 1765 (1990).
[22] G. G. Batrouni and R. T. Scalettar, Phys. Rev. Lett. **84** 1599 (2000).